



Investigating the impact of internal fatigue crack propagation in aluminum alloy plates repaired with a composite patch

Mohammed Chaib^{1,2} · Abdelkader Slimane^{3,4} · Sidahmed Slimane^{3,5} · Sidahmed Dahmane⁶ · Anas Abderrahmane Lahouel¹ · Djafar Ait Kaci⁶ · Kaddour Bahram^{2,4} · Habib Achache⁷ · Abdelkader Ziadi² · Benattou Bouchouicha⁴

Received: 24 October 2023 / Accepted: 19 January 2024 / Published online: 30 January 2024
© The Author(s), under exclusive licence to Springer-Verlag London Ltd., part of Springer Nature 2024

Abstract

The application of the Factor of Intensity of Constraint (FIC) criteria becomes instrumental in quantifying effectiveness by measuring the reduction in mechanical energy at the fracture tip, thereby extending the structural life. The robust mechanical properties offered by bonded composite patch repair technology, including enhanced fatigue resistance, mass gain, adaptability to complex sections, and corrosion resistance, play a pivotal role in fortifying damaged structures. Our findings highlight the interdependence of geometric and mechanical properties among the composite patch, adhesive, and damaged structure. Our investigation centers on M(T) aluminum alloy 6061 T6 centrally fissured samples from the 6000 series. We present a comprehensive examination of the effect of composite patch repairs on fatigue deterioration in aeronautical structures. Significantly, our study introduces novel insights by examining the effects of both constant and varying amplitude loads, emphasizing the contribution to comprehensive exploration that highlights the practical implications and benefits of composite patch repairs in enhancing fatigue resistance and longevity in aeronautical structures. Additionally, a detailed exploration is conducted to understand the effects of various parameter settings and service terms. This study contributes significant insights into the field, shedding light on the practical implications of composite patch repairs in enhancing the fatigue resistance and longevity of aeronautical structures.

Keywords Fatigue · Crack propagation · Patch · Aluminum alloy · Composite materials

✉ Abdelkader Slimane
aek.slimane@univ-usto.dz

¹ University of Ahmed, Ben Bella Oran 1, ISTA, B.P 1524, El M'Naouer, 31000 Oran, Algeria

² Laboratory of Intelligent Structures/DGRSDT, CTR University of Ain Temouchent, 46000 Ain Temouchent, Algeria

³ Laboratory of Applied Mechanics, Department of Mechanical Engineering, University of Sciences and Technology of Oran Mohamed Boudiaf, USTO-MB, El M'naouer, BP 1505, 31000 Oran, Algeria

⁴ Laboratory of Materials and Reactive Systems (LMSR), Department of Mechanical Engineering, University of Sidi-Bel-Abbes, Cité Ben M'hidi, Bp 89, 22000 Sidi Bel Abbes, Algeria

⁵ Centre of Satellite Development (CDS), Ibn Rochd USTO, BP.: 4065, Oran, Algeria

⁶ Faculty of Technology, University of Sidi-Bel-Abbes, Cité Ben M'hidi, Bp 89, 22000 Sidi Bel Abbes, Algeria

⁷ University of Oran2, Oran, Algeria

1 Introduction

Aeronautical structures made of aluminum alloy are subjected to fluctuating stresses while in service, such as pressurizations, pilot maneuvers, and atmospheric turbulence, which over time generates the phenomenon of fatigue [1–4], which modifies the properties localization of material and leads to the formation of cracks that propagate and lead to rupture, with fatigue accounting for 90% of structural failure [5–8].

For aeronautical constructions, internal cracks can be particularly dangerous since they can suddenly break catastrophically [9–11].

Internal cracks are those that are below the surface of the material or inside the structure, making them invisible to the unaided eye. They can develop for a number of reasons, including vibrations, fatigue loads, temperature variations, thermal cycles, debris hits, and manufacturing mistakes [9, 10, 12] (Fig. 1).

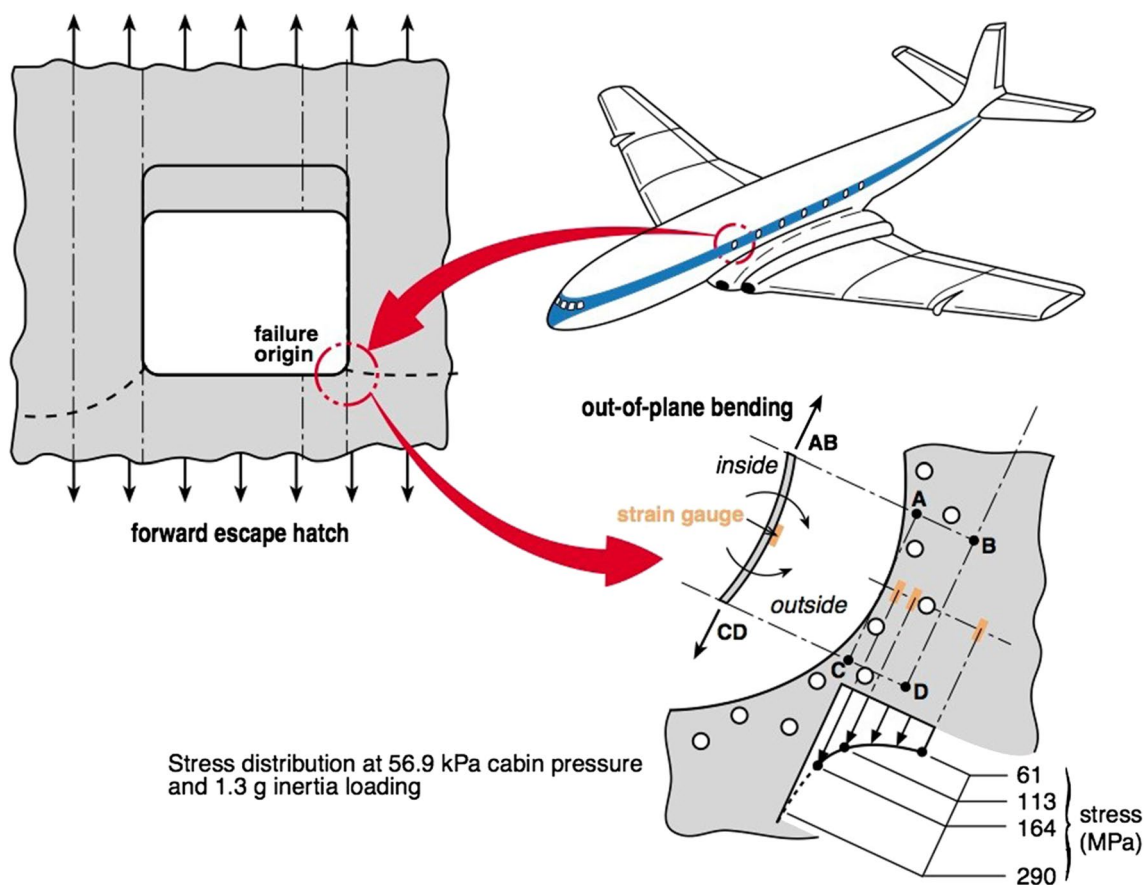


Fig. 1 Possible interior crack caused by aircraft stress

These fractures can widen and lead to structural failure if they are not found and fixed in a timely way. As internal cracks are not visible to the unaided eye, they might be challenging to find. Internal fractures in aeronautical structures can be found using non-destructive examination methods such as radiography, X-ray tomography, thermography, and ultrasound [13].

Depending on their size [14–16], location, and effect on the structure, internal fractures can be repaired with using different techniques including patch repair [17, 18] or friction stir welding [19].

Patch repair application in industry and aircraft airplane is used to repair localized damage or defects in structures such as composite materials [20, 21], metals, and alloys [22, 23]. In industry [24, 25], patch repair is used in various applications such as repairing pipelines, tanks, and pressure vessels [26, 27]. For example, if a pipeline has a localized defect, a patch can be applied over the damaged area to restore its strength and prevent leakage. Similarly, in tanks or pressure vessels, a patch can be applied to repair any cracks or damage [26, 27].

In aircraft airplane, patch repair is used to repair damage to the aircraft's structure, including the wings, fuselage, and

tail [28–30]. Patch repair can be used for both minor and major damage, depending on the severity of the damage [28, 29]. The patches used in these repairs are typically made from the same or similar materials as the original structure, such as composite materials or aluminum alloys [31].

Fazaz et al. studied the effect of plasticity on fatigue fracture formation in aluminum plates fixed with composite patches under single loading. The results showed a considerable increase in fatigue life, which was attributed to overload rather than the composite patch [32].

Yubo et al. investigated the reliability of unidirectional static load composite laminate patch repaired structures by developing a proxy model for maximum load capacity, taking into account repair material properties and design [33–35], incorporating probability distributions for random parameters, and conducting reliability and sensitivity analyses emphasizing the model's significance for subsequent design and evaluation of composite repaired structures [36].

Monika et al. developed a three-dimensional energy-based progressive degradation model for patch-repaired laminates that include shear non-linearity under tensile pressure. They analyzed the failure strengths of various pristine, drilled, and double-sided patch-repaired specimens [37].

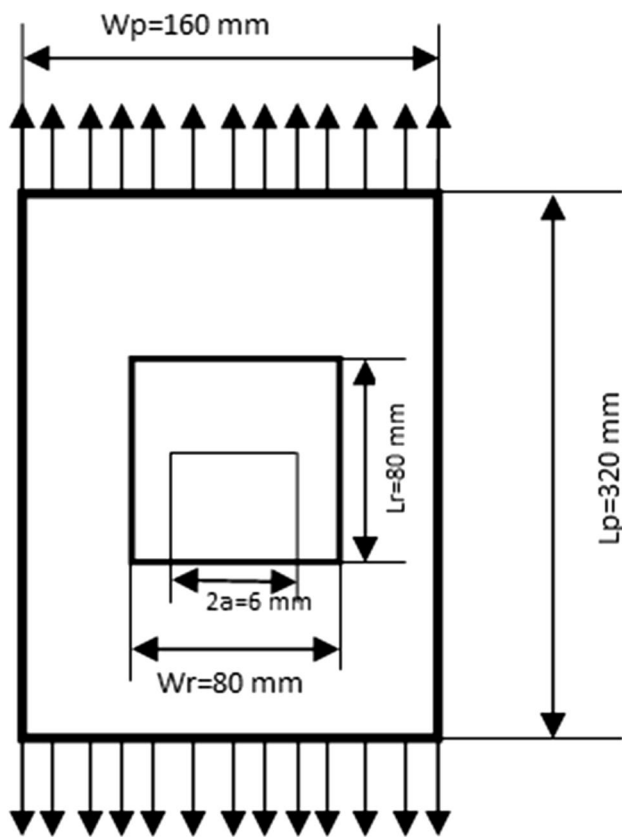


Fig. 2 Geometric model

The primary goal of this research is to investigate the influence of crack propagation on 6061T6 aluminum alloy plates repaired using composite patch under various cyclic loading conditions (constant and varied amplitude). We carried out a rigorous investigation on the case of an internal crack to understand the consequences of various parameter settings and service terms with solicitation conditions that are close to reality [38].

2 Material mechanical characteristics and geometric model

The patch-repaired aluminum alloy cracked specimen’s shape and measurements are depicted in Fig. 2. The plate has a nominal thickness of 3 mm, a length of 320 mm, and a width of 160 mm. At the margin of each specimen, there is an initial interior crack that is $2a = 6$ mm long. A composite patch with the following measurements is bonded to the damaged area of the plate: 80 mm in length, 80 mm in width, and 2 mm in thickness make up this structure.

Aluminum alloy 6061-T6 was the material employed in this investigation. In Table 1, the alloy’s mechanical characteristics are listed.

Table 1 Mechanical properties of 6061 T61

$\bar{\sigma}_c$ (MPa)	E (GPa)	KC (MPa√m)	KI_c (MPa√m)
282.685	68,947.6	39.558	28.57

Table 2 Mechanical properties of patch

	Boron/epoxy	Graphite/epoxy	Glare
E11	208	134	71
E22	25.4	10.3	71
E33	25.4	10.3	-
G12	7.2	5.5	344
G13	7.2	5.5	-
G23	4.9	3.2	-
ν_{12}	0.1677	0.33	0.3
ν_{13}	0.1677	0.33	0.3
ν_{23}	0.035	0.33	-

Table 3 Mechanical properties of adhesives

Adhesive	Ga (MPa)
FM-73	0.413
MB1113	0.848
3MAF163-2K	1.100

Boron/epoxy, graphite/epoxy, and glare are used for patch healing (Table 2).

The bonding adhesives used are MB1113, FM-73, and 3MAF163-2K (Table 3).

Figure 3 displays the dimensions and mechanical characteristics of the FM adhesive-73.

In symmetry, there are six plaices (Fig. 4). The plate under consideration is stretched in tension in the direction of opening mode (Mode I) at a maximum stress of 100 MPa.

Table 4 shows the characteristics of the fatigue propagation model for the aluminum alloy 6061 T6.

3 Results and analysis

3.1 Loading with a constant amplitude

3.1.1 Effect of ratio load

The impact of the load ratio on the cracking length m as a function of the number of cycles N is depicted in Fig. 5. Three load ratios are used in this work: $R = 0.1, 0.2,$ and 0.3 . It is evident that lengthening the fatigue life improved the load ratio. As a result of this rise, the load amplitude, $a = (\max - \min)$, decreases. These loads have corresponding amplitudes of 90, 80, and 70 MPa. The life to failure rose

Fig. 3 Patch dimensions and adhesive properties

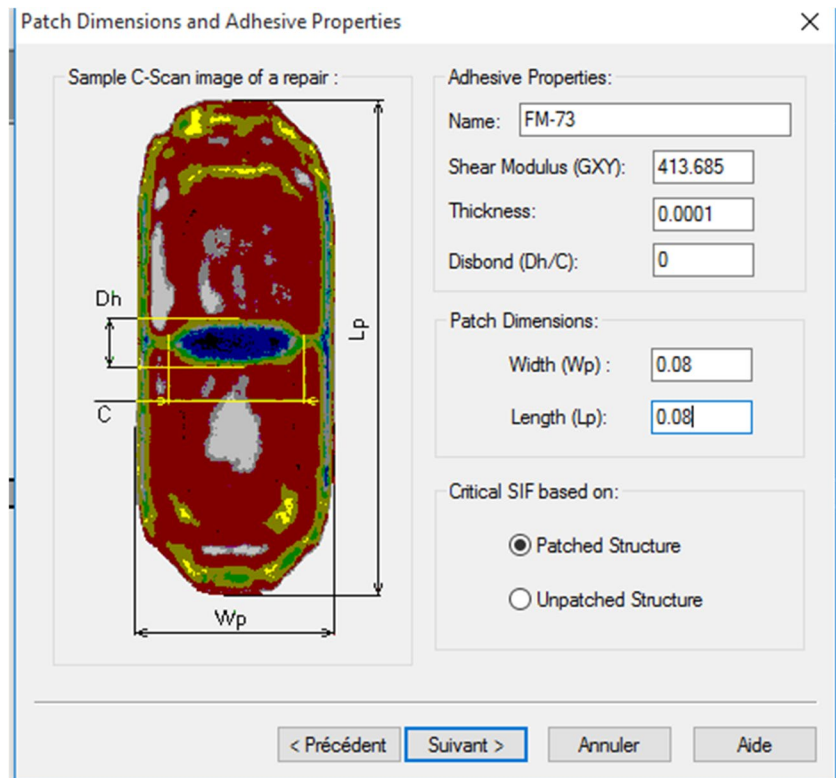


Fig. 4 Ply orientations and designed patch properties

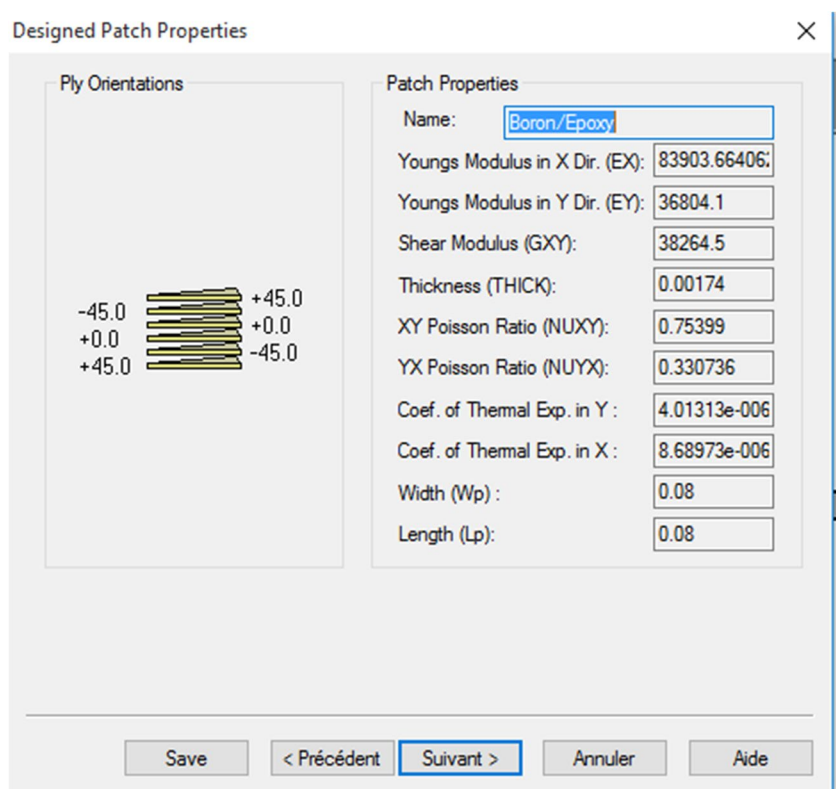


Table 4 Paramètre du modèle de propagation de l’alliage 6061 T6

C	N	p	q
1.84×10^{-9}	2.3	0.5	0.5

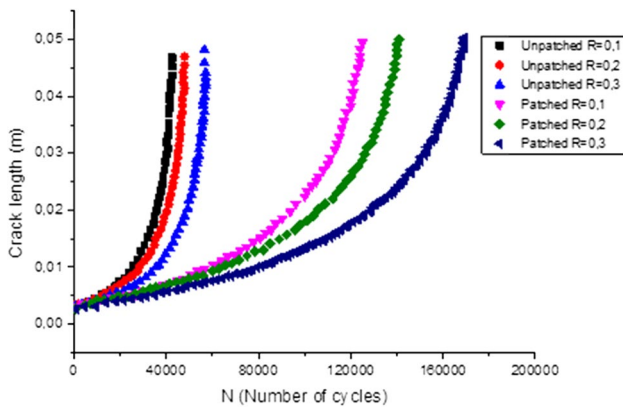


Fig. 5 Influence of load ratio on the fatigue life of a repaired and unrepaired boron/epoxy component

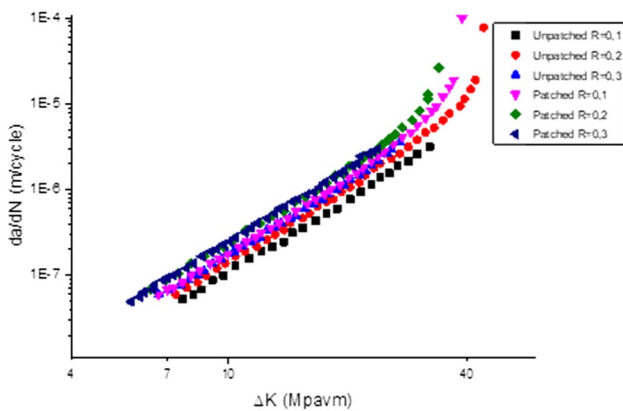


Fig. 6 Effect of load ratio on cracking rate for a boron/epoxy repaired and unrepaired portion

from 124,600 cycles to 168,600 cycles when the load was decreased from 90 to 70 MPa, which is equivalent to an increase rate of 1.35 times. Furthermore, when compared to the unrepaired specimen, the presence of the repaired patch extended the specimen’s life.

On the evolution of the cracking rate (propagation), the effect of the load ratio on fatigue cracking is clearly visible. The evolution of the cracking rate da/dN as a function of the amplitude of the stress intensity factor K is depicted in Fig. 6. The acquired result confirms the trend of the experimental data from the literature [39]. The cracking rate increases as the load ratio increases. The influence of the load ratio is more pronounced at the non-cracking threshold and/or at the beginning crack level.

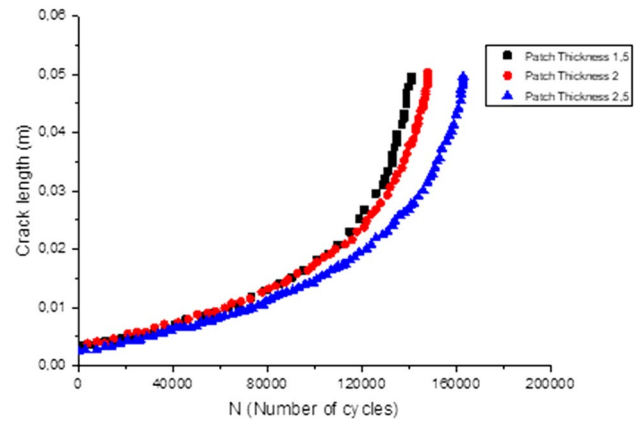


Fig. 7 Influence of patch thickness on fatigue life

The first stress intensity factor is decreased for the same initial fracture when the load ratio is increased. For a load ratio of $R = 0.1$, $K = 7.36$ MPa/m, while for $R = 0.3$, $K = 5.91$ MPa/m. For $R = 0.1$ to $R = 0.3$, K decreases from 30.8 m to 23.5 MPa m at high stress intensity values and the same cracking rate, respectively. There is an increase in the cracking rate for a given stress intensity component. In the case of $k = 20.4$ MPa, for instance, the cracking rate for $R = 0.1$ is 1.13×10^{-6} m/cycle and for $R = 0.3$, it is 1.77×10^{-6} , which corresponds to an increase rate of 36.15%.

3.1.2 Effect of patch thickness

The thickness of the patch represents an important parameter when repairing cracks and improving the stiffness of the cracked structure. Figure 7 shows the influence of the thickness of the patch on the fatigue life; the different thicknesses of the patches are $ep = 1.5$ mm, $ep = 2$ mm, and $ep = 2.5$ mm. It can be seen that increasing the thickness for the same number of ply increases the fatigue life. For thickness = 1.5 mm with a length of 49.29 mm, the number of breaking cycles is 140,300 cycles. For thickness = 2 mm with a length of 49.69 mm, the number of rupture cycles is 148,100 cycles. For thickness = 2.5 mm with a length of 50.02 mm, the number of breaking cycles is 162,900 cycles.

The stress intensity factor for the specimen repaired by a patch is shown in Fig. 8 evolving as a function of the fracture length under the influence of the patch’s thickness. It is observed that a 50 mm increase in patch thickness results in an 11.39% drop in stress intensity factor for the same number of ply. Below 10 mm in crack length, the evolution of the stress intensity factor is nonlinear. Beyond this length, the evolution of the stress intensity factor is almost linear (stable evolution).

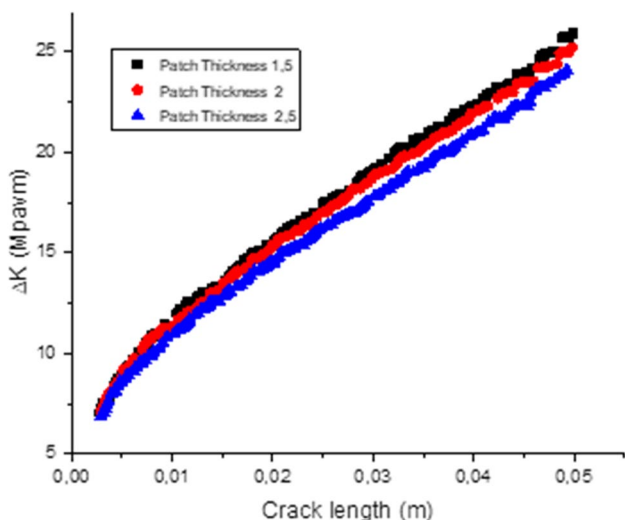


Fig. 8 Influence of patch thickness on intensity factor variation

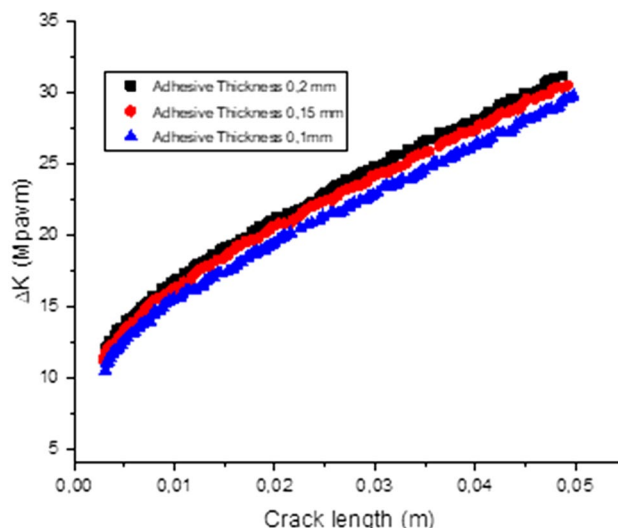


Fig. 10 Influence of adhesive thickness on variation of stress intensity factor

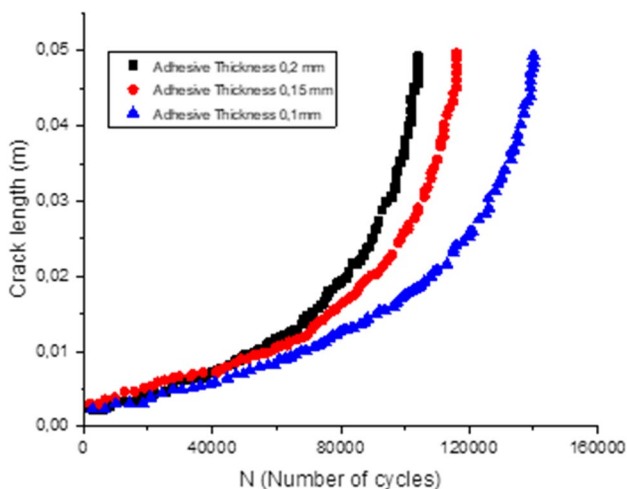


Fig. 9 Influence of adhesive thickness on fatigue life

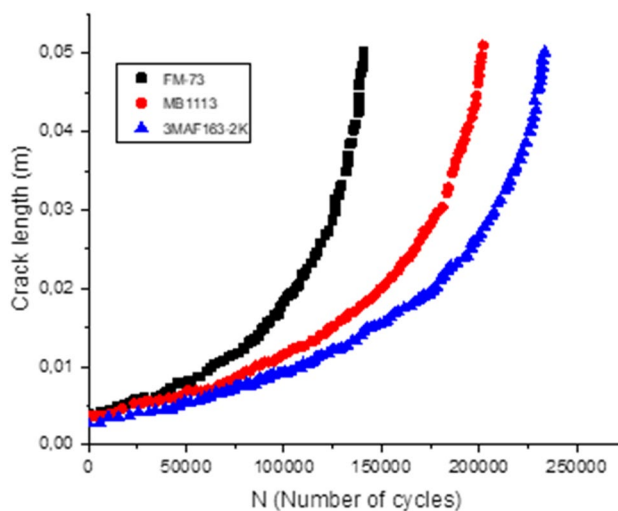


Fig. 11 Effect of adhesive type

3.1.3 Effect of adhesive thickness

In determining the durability of patch-reinforced cracks, the adhesive’s thickness is crucial. Figure 9 illustrates how adhesive thickness affects the fatigue life of the patched area. We tried several different thicknesses: 0.1 mm, 0.15 mm, and 0.2 mm. For $e_{pa}=0.1$ mm, the number of rupture cycles is 140,100 cycles; for $e_{pa}=0.15$ mm, the number of rupture cycles is 116,600 cycles, and for $e_{pa}=0.2$ mm is 103,400 cycles. It is noted that the reduction in thickness increases the fatigue life.

Figure 10 shows the effect of adhesive thickness on the stress intensity factor as a function of crack length. For $e_{pa}=0.1$ mm, the final crack is length $a=40$ mm, and the intensity factor is $\Delta k=21.2$ MPa \sqrt{m} . For $e_{pa}=0.15$ mm, the final crack length is $a=40$ mm, and the intensity factor

is $\Delta k=23.2$ MPa \sqrt{m} . And for $e_{pa}=0.2$ mm, the final crack length is $a=40$ mm, and the intensity factor is $\Delta k=23.9$ MPa \sqrt{m} . Reducing the thickness of the adhesive decreases the stress intensity factor at length $a=40$ mm to 11.29% and increases the number of cycles from 3.67×10^4 to 26.19%. This shows that the best performance of the adhesive is for the low thicknesses of the latter.

3.1.4 Influence of adhesive type

The characteristics of the adhesive type also have a significant impact on how stable patch-reinforced cracks are. Figure 11 illustrates the relationship between the type of

adhesive and the influence of the number of cycles on the variation in crack length. At the same crack length, $a = 50$ mm, we note that the FM-73 adhesive’s final cycle number was 140,300 cycles, the MB1113 adhesive’s final cycle number was 202,200 cycles, and the 3MAF163-2K adhesive’s final cycle number was 233,100 cycles. It is noticed that the lifetime of 3MAF163-2K is great with an increase rate of 39.98% compared to FM-73 and 13.25% compared to MB1113.

The relationship between the variation in stress intensity factor (SIF) and fracture length is shown in Fig. 12 as a result of the adhesive type. The shear modulus of the adhesive affects how strong the bonded patch is. Note that for the length of $a = 50$ mm, the type FM-73 the intensity factor $\Delta k = 27.2 \text{ MPa}\sqrt{\text{m}}$. For type MB1113, the intensity factor $\Delta k = 22.9 \text{ MPa}\sqrt{\text{m}}$, and for type 3MAF163-2K, the intensity factor $\Delta k = 21 \text{ MPa}\sqrt{\text{m}}$. When the 3MAF163-2K adhesive is utilized instead of the FM73 and MB1113 adhesives, the stress intensity factor is decreased by 22.79% and 8.29%, respectively. The stress intensity factor (SIF) falls as the shear modulus increases.

Analysis of this finding suggests that, in comparison to other adhesive types, the high shear modulus adhesive type 3MAF163-2K efficiently transfers load to the targeted part during repairs. As a result, the degree of stress is reduced and the duration of fatigue is increased.

3.1.5 Effect of patch nature

The nature of the patch’s material has an impact on stress intensity factor in addition to the effect of the patch’s thickness, nature, and thickness of the adhesive. Three materials were employed, including graphite/epoxy, boron/epoxy, and glare.

and glare, to demonstrate how the patch material affected the variance of the stress intensity factor KI. The effect of patch material on crack length is shown in Fig. 13 as a function of life at length $a = 50$ mm for graphite/epoxy and glare adhesives, both of which have the same final cycle number of 153,900 cycles, and for the adhesive boron/epoxy, which has a final cycle number of 162,900 cycles. We can see that the boron/epoxy provides a long life.

Figure 14 depicts the evolution of the stress intensity factor as a function of crack length as influenced by the composite patch materials used. We note at length $a = 50$ mm that for the graphite/epoxy and glare materials, the intensity factor is $\Delta k = 25.6 \text{ MPa}\sqrt{\text{m}}$, and for boron/epoxy, the intensity factor is $\Delta k = 24.1 \text{ MPa}\sqrt{\text{m}}$. The results reveal that

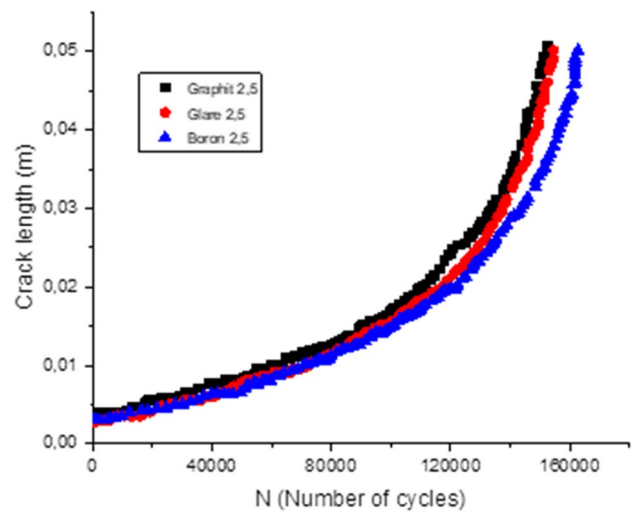


Fig. 13 Influence of patch material on fatigue life

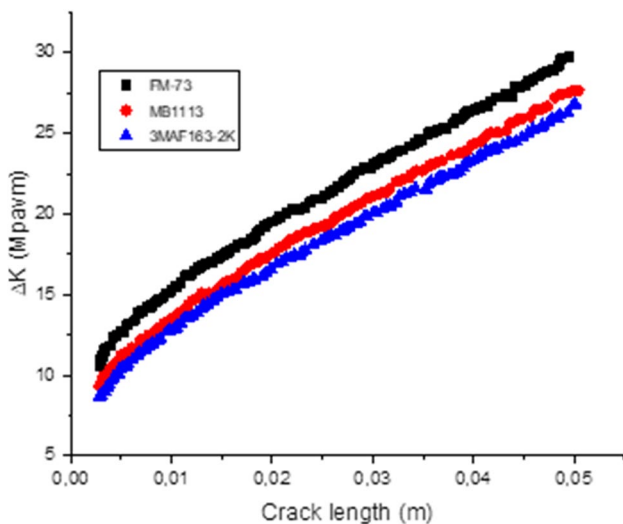


Fig. 12 Effect of adhesive type on variation of stress intensity factor

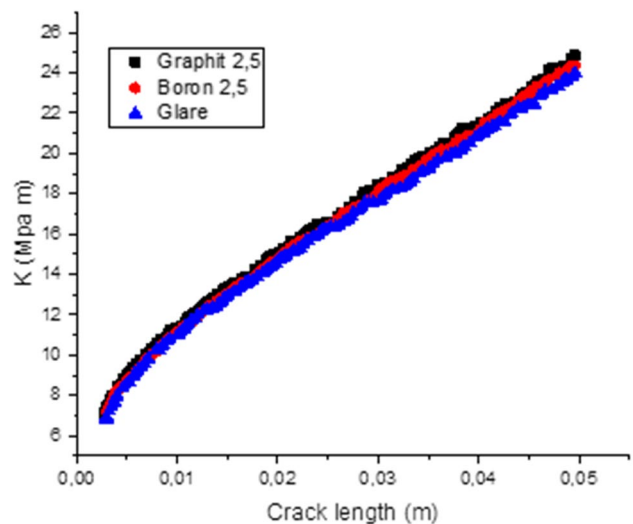


Fig. 14 Influence of patch material on variation of stress intensity factor

when boron/epoxy is used, the stress intensity factor is lower than when graphite/epoxy and glare are used. It is noted that the nature of the boron/epoxy patch is a better performance in terms of resistance to rupture.

3.1.6 Effect number of ply

The amount of adhesive plies is critical to the stability of patch-reinforced cracks. Figure 15 illustrates how the amount of plies affects the fatigue life of the patch that has been fixed. The different ply counts of the patches are 6 ply, 8 ply, and 10 ply. It can be seen that the increase in the number of plies for the same thickness $e_p = 1.5$ mm increases the fatigue life. At length $a = 50$ mm for 6 plies, the final cycle number is 140,400 cycles. For 8 plies, the final cycle count is 144,000 cycles. For 10 plies, the final cycle number is 149,700 cycles.

The difference in the number of plies for the same thickness increases the number of final cycles, and the increase in oriented fibers reinforces and restricts the crack [40].

3.2 Variable loading

3.2.1 Effect of overload

Figures 16 and 17 show respectively the comparison of fatigue life and cracking rates between repaired and unrepaired aluminum alloy 6061 T6 plate under the application of constant amplitude loading with a single overload ($\tau = 2.2$). For the unrepaired plate, the number of rupture cycles is 6.104 cycles in the presence of overload. Note the existence of a delay level [41]. The number of cumulative delay cycles is 165,735 cycles. The repair by patch in the presence of variable loads (overloads) contributed to the

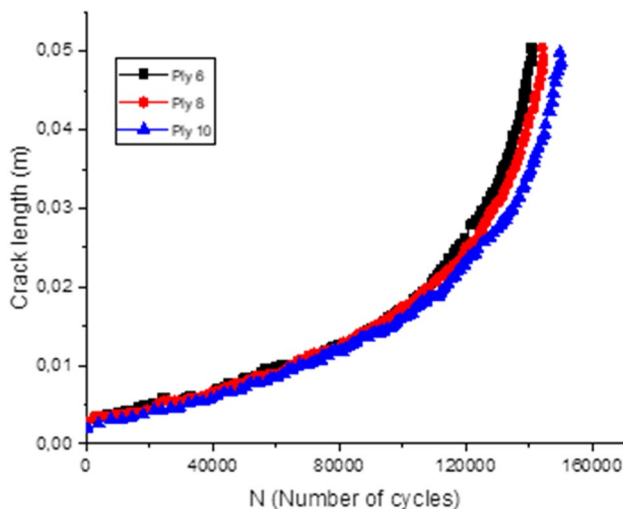


Fig. 15 Effect of patch pliance number on fatigue life

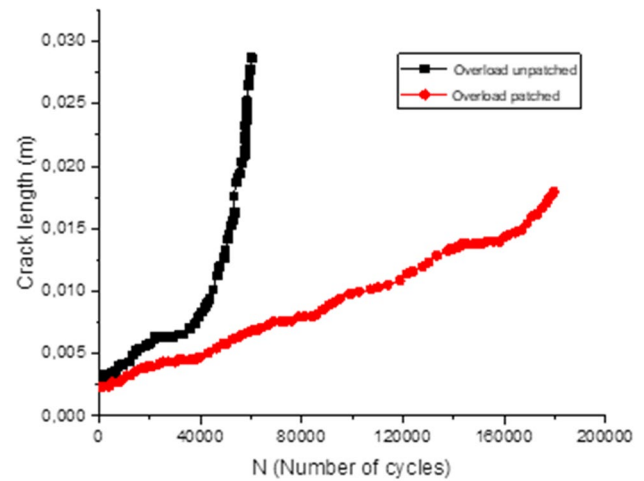


Fig. 16 Influence of single overload on the fatigue life

increase in the fracture life and reached a number of fracture cycles of 1.8×10^5 cycles. The difference in lifetime accumulated by the application of repair by patch is 1.2×10^5 cycles. During the propagation, there are four stages of delay due to the repetitions of the application of the overloads. The rate of improvement due to the combined effects of patch repair and the application of overloads is 65.82%. The rupture length reached in the presence of the patch is 18 mm; on the other hand, the final rupture length of the unrepaired specimen is 28 mm.

Figure 17 compares the rates of cracking in the repaired and unrepaired plates under varying loads for $\tau = 2.2$. For the case of the unrepaired plate, one notes the presence of a type of delay, an immediate delay (instantaneous) at crack length “ $a = 6.61$ mm.” Its reduction speed is 1.05×10^{-7} m/cycle. We usually take note of the three forms of interaction delays

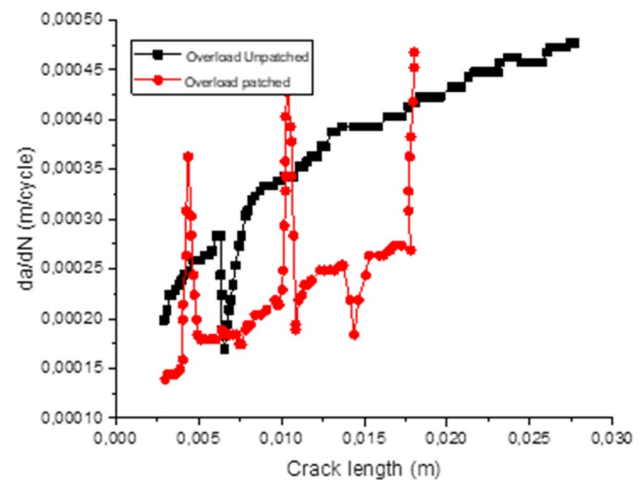


Fig. 17 Effect of patch repair (boron/epoxy) under the application of an overload on the cracking rate

in the case of the mended plate. The first is an immediate acceleration at fracture length $a=4.37$ mm. The second is an immediate delay with a speed of 9.29×10^{-8} at a length of 14.45 mm, while the third is a delayed delay with a speed that reaches a maximum at 1.47×10^{-6} m/cycle before decreasing to 1.05×10^{-7} m/cycle.

3.2.2 Effect of overload rate

Figure 18 shows the effect of different overload rates on the fatigue life of the patch-repaired specimen. According to the data, patch repair increases fatigue life for various overload rates. The presence of delay levels is observed. The lifetime caused by the delay is of the order of 4.2×10^4 cycles. The effect of repair by patch is more significant for an overload rate “ $\tau=2.2$.” The number of delay stages is increased and consequently the life at break. The difference in lifetime for “ $\tau=2.2$ ” compared to constant amplitude loading for $R=0.2$ is 9×10^4 cycles. This represents an increase rate of 39.13%.

3.3 Overload band effect

Figure 19 shows the influence of variable block loading on the life and cracking rate of the M(T) plate repaired by boron/epoxy in aluminum alloy 6061T6. Two types of cyclic loading blocks are applied named L–H block and H–L block. Comparing the loading of constant amplitude for $R=0.35$ and the block of cyclic loadings “L–H,” it can be seen that the application of the cyclic loading by block “L–H” increased the residual life of the plate fissured and repaired by patch. This increase is of the order of 60,266 cycles and 13,242 cycles, respectively, compared to the cyclic loading with constant amplitude and the loading “L–H.” It is noted that the application of the H–L block reduces the fatigue life,

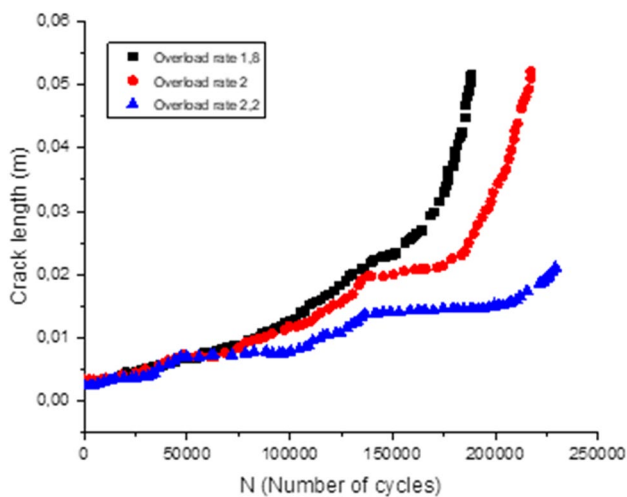


Fig. 18 Effect of different overload rate on patch repaired specimen fatigue life

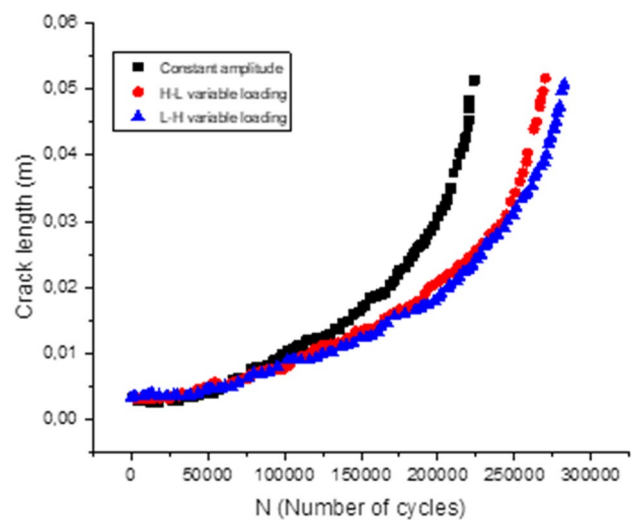


Fig. 19 Effect of different overload band on repaired specimen fatigue life

and it is noted that the difference in the fatigue life of the two blocks “H–L” and “L–H” are very small. The effects of applying “L–H” and “H–L” blocks are more significant at the start of cracking. One notes for the block “L–H” a weak speed at the beginning of cracking compared to the speed for a loading with constant amplitude $R=0.35$ the speed at the beginning of cracking is of the order of 2.82×10^{-8} m/cycle is increased abruptly at 5.83×10^{-8} m/cycle after the application of the “H” loading of the “L–H” block, and it reaches the cracking rate due to the constant amplitude loading $R=0.35$. The application of the “H–L” block indicates that at the start of cracking, the speed takes on the appearance of the loading cracking speed at a constant amplitude $R=0.35$. After the duration of application of the “H” loading of the “H–L” block, which is 40,000 cycles, the cracking speed is reduced and has increased from 6.29×10^{-8} m/cycle to 4.42×10^{-8} m/cycle. The results also indicate that the duration of the blocks at the start of cracking “ $N=40,000$ cycles” affects the residual lifetimes and the cracking speeds.

4 Conclusion

The research focuses on the use of patch repair in the aerospace industry [42], specifically for treating localized damage in 6061T6 aluminum alloy plates with constant amplitude and varied loading. The research takes into account patch and adhesive qualities, as well as load-related parameters. Overload rate, delay model, overload application, and load ratio are all considered in the analysis. The findings revealed that.

- The effect of applying the composite patch for repair and increasing the load ratio extended the fatigue life and reduced the stress intensity factor.
- The effect of increasing the thickness of the patch resulted in an extension of life and reduction of FIC.
- Improved fatigue life and reduced FIC due to reduced adhesive thickness.
- The high shear modulus adhesive type 3MAF163-2K results in good load transmission to the part to be repaired, therefore increasing the fatigue life and reducing the stress intensity factor.
- Boron/epoxy offers better resistance to breakage compared to other repair materials.
- The reinforcement of the composite patch through an increase in oriented fibers serves to restrict crack propagation.
- Patch repair under variable loading with a single overload increased fatigue life and reduced cracking speed.
- The variation of overload rate extended the delay life, and the analysis of the cracking speed curves reveals two types of delay: instantaneous delay and deferred delay.
- The application of the different models on the repaired part showed that the Willenborg model gave a significant speed reduction rate.
- The increase in delay rate increased the number of final cycles and delayed the cracking rate.—The “H–L” loading increased the fatigue life compared to the “L–H” loading and the “ $R=0.35$ ” loading, and the onset of cracking makes it possible to increase the cracking rate at the constant amplitude loading rate.
- The “L–H” loading has a small effect on the fatigue life, and the cracking rate is reduced after the application of the “H” block of the “L–H” loading. Finally, the combination between repair by patch and the application of loads with overloads offers a high resistance to fatigue failure (increases the life of the structure).

Author contribution Mohammed Chaib: writing, reviewing and editing.

Abdelkader Slimane: conceptualization, methodology, writing.

Sid-Ahmed Slimane: formal analysis.

Sidahmed Dahmane: supervision.

Anas Abderrahman Lahouel: supervision.

Djafar Ait Kaci: writing, formal analysis.

Kaddour Bahram: reviewing.

Habib Achache: supervision.

Abdelkader Ziadi: supervision, investigation, data curation.

Benattou Bouchouicha: supervision, data curation.

Data availability Not applicable.

Code availability Not applicable.

Declarations

Ethics approval Not applicable.

Consent to participate Not applicable.

Conflict of interest The authors declare no competing interests.

References

1. Slimane A, Bouchouicha B, Benguediab M, Slimane SA (2015) Contribution to the study of fatigue and rupture of welded structures in carbon steel-a48 ap: experimental and numerical study. *Trans Indian Inst Met* 68:465–477
2. Slimane A, Bouchouicha B, Benguediab M, Slimane SA (2015) Parametric study of the ductile damage by the Gurson–Tvergaard–Needleman model of structures in carbon steel A48-AP. *J Market Res* 4:217–223
3. Lahouel AA, Mekidiche M, Belmir C, Slimane A, Sahli N (2023) Synthesis and characterization of poly (vanillin pyrrole)/zinc oxide composite for photocatalysis application under natural sunlight irradiation. *Polymer Science, Series B*, pp 1–9
4. Belhadj M, Lahbari N, Slimane A, Aouiche D (2020) An interactive method to analysis of the response of the different reinforcement structures of a door opening of a wind tower. *Period Polytech Mech Eng* 64:263–272
5. Hertzberg RW, Hauser FE (1977) Deformation and fracture mechanics of engineering materials. *J Eng Mater Technol* 99(1):96
6. Kessinger RH (2001) Structural health monitoring of aerospace composite structures. *J Aerosp Eng* 14:18–23
7. Chaib M, Megueni A, Ziadi A, Guagliano M, Belzunze FJV (2016) Experimental study of the shot peening treatment effect on austenitic stainless steel. *Int J Mater Prod Technol* 53:298–314
8. Chaib M, Slimane A, Slimane SA, Ziadi A, Bouchouicha B (2021) Optimization of ultimate tensile strength with DOE approach for application FSW process in the aluminum alloys AA6061-T651 & AA7075-T651. *Frattura ed Integrità Strutturale* 15:169–181
9. Nicholas T (1999) Aircraft structural life assessment. *J Aircr* 36:37–46
10. Baker AA (2004) Composite materials for aircraft structures. AIAA
11. Lebbal H, Chaib M, Slimane A, Ait Kaci D, Boualem N (2023) Experimental investigation with optimization of spot welding parameters on stainless steel AISI 304. *JOM* 75(11):4993–5002
12. Blakey-Milner B, Gradl P, Snedden G, Brooks M, Pitot J, Lopez E et al (2021) Metal additive manufacturing in aerospace: a review. *Mater Des* 209:110008
13. Slimane A, Chaib M, Slimane S, Dahmane S, Lahouel A A, Guelailia A, Bahram K, Kebdani S, Bouchouicha B (2024) Mechanical behavior of carbon fiber-reinforced plastic during rotary ultrasonic machining. *Int J Adv Manuf Technol* 1–13
14. Dahmane S-A, Azzedine A, Megueni A, Slimane A (2019) Quantitative and qualitative study of methods for solving the kinematic problem of a planar parallel manipulator based on precision error optimization. *Int J Interact Des Manuf* 13:567–595
15. Dahmane SA, Megueni A, Azzedine A, Slimane A, Lousdad A (2019) Determination of the optimal path of three axes robot using genetic algorithm. *Int J Eng Res Afr* 44:135–149
16. Kadem M, Semmah A, Wira P, Slimane A (2020) Artificial neural network active power filter with immunity in distributed generation. *Period Polytech Mech Eng* 64:109–119

17. Rose L (1982) A cracked plate repaired by bonded reinforcements. *Int J Fract* 18:135–144
18. Her SC, Shie DL (1998) The failure analysis of bolted repair on composite laminate. *Int J Solids Struct* 35:1679–1693
19. Salami P, Khandani T, Asadi P, Besharati M (2014) Friction stir welding/processing as a repair welding. *Advances in Friction-Stir Welding and Processing*, pp 427–457
20. Hosseini-Toudeshky H, Mohammadi B, Bakhshandeh S (2006) Fatigue crack trajectory analysis of single-side repaired thin aluminum panels with various composite patch lay-up configurations. III European Conference on Computational Mechanics: Solids, Structures and Coupled Problems in Engineering. *Book of Abstracts*, pp 429–429
21. Su W, Zou L, Mu Z, Li X (2014) Stress analysis of cracked metallic aircraft structure adhesively repaired with composite patch. *Proceedings of the First Symposium on Aviation Maintenance and Management Volume II:369–377*
22. Balakrishnan VS, Seidlitz H (2018) Potential repair techniques for automotive composites: a review. *Compos B Eng* 145:28–38
23. Rider AN, Arnott DR, Mazza JJ (2018) Surface treatment and repair bonding. *Aircraft Sustainment and Repair*. Elsevier, pp 253–323
24. Slimane A, Kebdani S, Bouchouicha B, Benguediab M, Slimane S, Bahram K et al (2018) An interactive method for predicting industrial equipment defects. *Int J Adv Manuf Technol* 95:4341–4351
25. Slimane S, Kebdani S, Boudjemai A, Slimane A (2018) Effect of position of tension-loaded inserts on honeycomb panels used for space applications. *Int J Interact Des Manuf* 12:393–408
26. Fazzini PG, Otegui JL (2006) Influence of old rectangular repair patches on the burst pressure of a gas pipeline. *Int J Press Vessels Pip* 83:27–34
27. Ali Ghaffari M, Hosseini-Toudeshky H (2013) Fatigue crack propagation analysis of repaired pipes with composite patch under cyclic pressure. *J Press Vessel Technol* 135
28. Okafor AC, Singh N, Enemuoh U, Rao S (2005) Design, analysis and performance of adhesively bonded composite patch repair of cracked aluminum aircraft panels. *Compos Struct* 71:258–270
29. Katnam KB, Da Silva L, Young T (2013) Bonded repair of composite aircraft structures: a review of scientific challenges and opportunities. *Prog Aerosp Sci* 61:26–42
30. Gu L, Kasavajhala ARM, Zhao S (2011) Finite element analysis of cracks in aging aircraft structures with bonded composite-patch repairs. *Compos B Eng* 42:505–510
31. Suman S, Dwivedi K, Anand S, Pathak H (2022) XFEM–ANN approach to predict the fatigue performance of a composite patch repaired aluminium panel. *Compos C: Open Access* 9:100326
32. Ahmed F, Mohammed S, Benyahia F, Bouiadjra BAB, Albedah A (2022) Plasticity analysis in aluminum alloy plates repaired with bonded composite patch under overload. *Proceedings of the 10th International Conference on Fracture Fatigue and Wear: FFW 2022*. Ghent University, Belgium, pp 21–27
33. Lahouel AA, Mekidiche M, Slimane A, Sahli N (2023) A comparative analysis of photocatalytic applications using poly [(vanillin-co-pyrrole)]/ZnO and TiO₂-based semiconductor under natural sunlight irradiation. *J Appl Polym Sci* 140:e54361
34. Kaddour B, Bouchouicha B, Benguediab M, Slimane A (2018) Modeling and optimization of a cracked pipeline under pressure by an interactive method: design of experiments. *Int J Interact Des Manuf* 12:409–419
35. Dahmane SA, Slimane A, Chaib M, Kadem M, Nehari L, Slimane SA et al (2023) Analysis and compensation of positioning errors of robotic systems by an interactive method. *J Braz Soc Mech Sci Eng* 45:119
36. Zhao Y, Hu K, Fu B, Wang Z, Wang Y, Yao X (2023) Reliability analysis of composite laminate patch repaired structures based on response surface proxy model. *Compos Commun* 42:101689
37. Kushwaha M, Bhatia GS, Arockiarajan A (2023) Nonlinear progressive damage model for woven patch-repaired laminate composites. *Compos Struct* 320:117154
38. Bahram K, Bouchouicha B, Benguediab M, Slimane A (2017) Admissibility of external cracks in a pipeline API X60 using the SINTAP procedure. *Period Polytech Mech Eng* 61:261–265
39. Albedah A, Khan SM, Benyahia F, Bouiadjra BB (2015) Experimental analysis of the fatigue life of repaired cracked plate in aluminum alloy 7075 with bonded composite patch. *Eng Fract Mech* 145:210–220
40. Slimane A, Slimane S, Kebdani S, Chaib M, Dahmane S, Bouchouicha B et al (2019) Parameters effects analysis of rotary ultrasonic machining on carbon fiber reinforced plastic (CFRP) composite using an interactive RSM method. *Int J Interact Des Manuf* 13:521–529
41. Bahram K, Chaib M, Slimane A, Bouchouicha B (2020) Simulation of the delay effect after applying a simple overload on alloys of aluminum 2024T351 using the Willemborg model. *Frattura ed Integrità Strutturale* 14:467–476
42. Slimane SA, Slimane A, Guelailia A, Boudjemai A, Kebdani S, Smahat A et al (2022) Hypervelocity impact on honeycomb structure reinforced with bi-layer ceramic/aluminum facesheets used for spacecraft shielding. *Mech Adv Mater Struct* 29:4487–4505

Publisher's Note Springer Nature remains neutral with regard to jurisdictional claims in published maps and institutional affiliations.

Springer Nature or its licensor (e.g. a society or other partner) holds exclusive rights to this article under a publishing agreement with the author(s) or other rightsholder(s); author self-archiving of the accepted manuscript version of this article is solely governed by the terms of such publishing agreement and applicable law.